Super-Poissonian Statistics of Photon Emission from Single CdSe-CdS Core-Shell Nanocrystals Coupled to Metal Nanostructures

Young-Shin Park, Yagnaseni Ghosh, Yongfen Chen, Andrei Piryatinski, Ping Xu, Nathan H. Mack, Hsing-Lin Wang, Victor I. Klimov, Jennifer. A. Hollingsworth, and Han Htoon

Phys. Rev. Lett. **110**, 117401 — Published 11 March 2013

DOI: 10.1103/PhysRevLett.110.117401

Super-Poissonian Statistics of Photon Emission from Single Core/Shell Nanocrystals Coupled to Metal Nanostructures

Young-Shin Park,[1,2] Yagnaseni Ghosh,[2] Yongfen Chen,[1,2] Andrei Piryatinski,[3] Ping Xu,[1] Nathan H. Mack,[1] Hsing-Lin Wang,[1] Victor I. Klimov,[1,4] Jennifer. A. Hollingsworth[2] and Han Htoon[1,2]

[1]Chemistry Division, Los Alamos National Laboratory, Los Alamos, New Mexico 87545, USA.

[2]Materials Physics & Applications: Center for Integrated Nanotechnologies, Los Alamos National Laboratory, Los Alamos, New Mexico 87545, USA.

[3]Theory Division, Los Alamos National Laboratory, Los Alamos, New Mexico 87545, USA.

[4]Center for Advanced Solar Photophysics, Los Alamos National Laboratory, Los Alamos, New Mexico 87545, USA.

We demonstrate that photon antibunching of individual nanocrystal quantum dots (NQDs) can be transformed into photon bunching (super-Poissonian statistics) when they are coupled to metal nanostructures (MNs). This observation indicates that, while the quantum yield of a biexciton (Q_{2X}) is lower than that of a single exciton (Q_{1X}) in free-standing NQDs, Q_{2X} becomes greater than Q_{1X} in NQDs coupled to MNs. This unique phenomenon is attributed to metal-induced quenching with a rate that scales more slowly with exciton multiplicity than the radiative decay rate and dominates over other nonradiative decay channels for both single excitons and biexcitons.

Strong electromagnetic fields associated with plasmons in metallic nanostructures (MNs) are known to enhance excitation and radiative recombination rates of proximal nanoemitters [1]. At the same time, they can also quench their photoluminescence (PL) by opening additional nonradiative decay channels [1]. The competition between PL enhancement and quenching has been studied extensively in a variety of nanoemitter-MN coupled systems. In the case of semiconductor nanocrystals quantum dots (NQDs), these studies have shown that coupling to MNs can lead to modifications of PL efficiency, decay dynamics [2,3] and PL blinking behaviors [4,5]. However, so far most of previous research has been conducted in the context of MNs interacting with single excitons.

Interactions of multiexcitons with MNs, however, can be significantly different from those in the single exciton regime (Fig. 1(a)). Specifically, plasmonic fields can modify not only the radiative rates of exciton (1X) and biexciton (2X) ($k_{1X,R}$ and $k_{2X,R}$), but also the nonradiative Auger recombination (AR) rate ($k_{2X,A}$). Further, while AR plays a dominant role in quenching the PL of multiexcitons in free-standing NQDs, metal-induced quenching of multiexciton PL can dominate over AR when NQDs are coupled to MNs, i.e., $k_{1X,M}$, $k_{2X,M} > k_{2X,A}$ where $k_{1X(2X),M}$ is metal-induced quenching rate of 1X (2X). These changes in radiative and nonradiative processes can modify PL quantum yields of single excitons and biexcitons (Q_{1X} and Q_{2X}, respectively) and can in turn influence the dynamics of the biexciton quantum cascade process. As the relationship between Q_{1X} and Q_{2X} plays a key role in defining the two-photon correlation function $g^{(2)}$ (Refs. [6] and [7]), NQD-MN interactions can lead to modifications in photon emission statistics (see Figs. 1(b) and 1(c), the corresponding figure captions and SI. 2).

To explore this exciting possibility of modifying photon emission statistics, we performed time resolved PL and photon correlation spectroscopy studies on 70 individual CdSe/CdS core/shell

NQDs. We observe that while all the NQDs on quartz substrates (reference NQDs) show incomplete photon antibunching like other single quantum emitters [8-10], more than 30% of individual NQDs coupled to silver nanoflakes exhibit *strong photon bunching* with the area ratio between the center peak and the side peak of second-order intensity correlation function ($g^{(2)}$) reaching as high as two. We further relate this dramatic behavior to a peculiar biexciton (2X)→ single-exciton (1X) recombination regime, in which Q_{2X} exceeds Q_{1X}. This condition is very unique because for reference NQDs, Q_{2X} is always observed to be much less than Q_{1X} due to multiexcitonic, nonradiative Auger recombination channels. Even in the complete absence of such multiexciton nonradiative decay channels, Q_{2X} is only expected to be equal to Q_{1X}. Finally, our analysis reveals that the strong photon bunching is impossible if metal quenching of the multiexciton PL is dominated by Förster resonance energy transfer from the NQD to the metal. Instead, it requires a nonradiative process that scales with the exciton occupation number (i.e. $k_{2X,M} = 2\ k_{1X,M}$). As these conditions can be satisfied in other nanoscale light emitters such as carbon nanotubes and epitaxially grown quantum dot, our work may inspire the development of a general plasmonic approach for manipulation of photon emission statistics. Such ability could bring breakthroughs in development of single-photon and/or entangled photon-pair sources that are critically needed for quantum communication applications [11]. In addition this work brings new understanding of multiexciton-MN interactions, which will aid in the development of new approaches for controlling multiexciton processes including those responsible for light amplification [12].

In this experiment we utilize a new type of core/shell NQD, in which a 3 nm diameter CdSe core is overcoated with an ultra-thick 18 monolayers CdS shell. In contrast to standard dots, these "giant" NQDs (g-NQDs) (here, diameter ~16 nm) are characterized by blinking-free PL [6,13] in

the spectral range of 600-650 nm and strong suppression of AR [14,15]. While the suppression of blinking makes g-NQDs more relevant for single-photon and photon-pair source applications, the AR suppression plays an important role in understanding the experimental observations reported below. Our g-NQDs were synthesized according to a modified literature procedure [13]. Time trajectories of PL emission, decay dynamics and $g^{(2)}$ functions of individual g-NQDs drop casted on either quartz substrates or silver nanoflakes films [16] were measured by performing a standard single-dot, time-resolved PL experiment (see SI for experimental details).

In Figs. 2(a) and 2(b), we compare $g^{(2)}$ functions and the PL decay (insets) of two g-NQDs, each of which is deposited on either a quartz substrate or a silver film. As expected, our data acquired at low pump power (the average NQD exciton occupancy $\langle N \rangle << 1$) [17] show that the PL decay dynamics of the g-NQD on the silver films (~0.9 ns time constant) is significantly faster compared to that on the quartz substrate (~39 ns time constant). Importantly, $g^{(2)}$ measurements reveal that the photon emission statistics transforms dramatically from an incomplete antibunching measured on the quartz to strong photon bunching for some g-NQDs coupled to the silver film. The degree of photon bunching (R), which we define as the area ratio between the center and the side peak of $g^{(2)}$, can reach the value of 2 at the lowest pump power. This low-intensity limit of R (referred below as R_0) varies widely for both reference g-NQDs and those on the sliver film. However, averaged R_0 (=0.90) observed for g-NQDs on the sliver film is enhanced by a factor of ~5.4 compared to that of reference samples (=0.17). About 30% of the g-NQDs on the silver film have R_0 values ≥1 (Fig. 2(c)).

Figure 2d shows that shorter PL decay times correspond to larger R_0s. This indicates a link between the photon bunching and the PL lifetimes in the NQDs. We have reported a wide

distribution in the R_0 values and PL lifetimes in free-standing g-NQDs [6] and attributed it to a wide variation in Auger lifetimes resulting from variations in the internal structure of the g-NQD [6,14]. Our analysis, presented later in the paper shows that this variation together with changes in the g-NQD-metal coupling are responsible for a fairly wide distribution of the R_0.

Figures 3(a)-(b) display $g^{(2)}$ functions measured from two different g-NQDs on a silver film for various values of $\langle N \rangle$. At the lowest $\langle N \rangle << 1$, the g-NQDs show R_0 = 1.7 and 1.2, respectively. Despite significant differences in the R_0 values, the degrees of photon bunching at higher pump powers exhibit similar $\langle N \rangle$ dependence (Fig. 3(c)). First, R gradually decreases with increasing $\langle N \rangle$ until it reaches a minimum at $\langle N \rangle \sim 0.2$ - 0.3. Then, R starts to increase until it asymptotically approaches unity for $\langle N \rangle >> 1$. The dip in the R vs. $\langle N \rangle$ dependence appears more pronounced for g-NQDs with $R_0 \sim 1$. In contrast, the R vs. $\langle N \rangle$ dependence of the reference g-NQDs exhibits a monotonous increase towards one (Fig. 3(c), triangles).

Strong photon bunching indicates that coupling to the metal leads to the situation where Q_{2X} is greater than Q_{1X} (Fig. 1(c)). This is the opposite of the situation in free-standing NQDs where Q_{2X} is usually much smaller than Q_{1X} due to fast AR. The realization of the condition $Q_{2X} > Q_{1X}$ first demands a reduction of Q_{1X} from near-unity values reported for reference g-NQDs [4,6]. Indeed, our analysis on distributions of PL intensities and average lifetimes for both the reference g-NQDs and the g-NQDs on silver films attained in the $\langle N \rangle < 1$ regime indicates that the enhancement in the nonradiative rate wins over that of the radiative rate and Q_{1X} is reduced on average to 0.13 of the original value (see SI. 5). However, this condition alone is not sufficient.

We have performed an analysis of the relation between Q_{2X} and $Q_{1X,}$ to derive other conditions

required to produce the regime of photon bunching. Since the rate of photon emission is defined by the number of radiative recombination pathways, the radiative decay rate of a multiexciton of the j^{th} order can be related to that of a single exciton using a statistical scaling, $k_{jX,R} = j^2\ k_{1X,R}$ [18,19]. Our theoretical analysis (SI. 6) shows that it is valid for plasmonically enhanced radiative processes. Next, we express the nonradiative rate due to metal quenching as $k_{jX,M} = j^{\gamma}\ k_{1X,M}$ where the value of γ varies depending on specific nature of the nonradiative process. With these two scaling relationships, we obtain $R_0 = (1+\alpha)/\left(1+\left(\frac{2^{\gamma}}{2^2}\right)\alpha+\frac{1}{2^2}\beta\right)$, where $\alpha = k_{1X,M}/k_{1X,R}$ and $\beta = k_{2X,A}/k_{1X,R}$ relate the rates of metal-induced quenching and AR to the single-exciton radiative decay rate. According to this expression, R_0 can become greater than unity only when γ is less than 2. Plots of R_0 vs. γ for different α and β values (Fi.g. 4(a)) clearly demonstrate this point. These calculations show that, in the case of $\alpha >> 1$ and $\alpha >> \beta$, R_0 can reach a value of 2 only when γ is equal to one, suggesting that the rate of metal induced nonradiative decay for mulitexcitons scales *linearly* with *j*.

Our calculations indicate that variations in α and/or β should lead to the spread in R_0 values (Fig. 2(c)). The inverse scaling between R_0 and the PL lifetime in Fig. 2(d) indicates that dot-to-dot variations in α indeed contribute to changes in R_0. However, when $\alpha < \beta$, AR dominates in defining R_0 and PL lifetimes. Therefore, in the limit of weak metal-induced quenching, both of these parameters should approach the values observed in reference g-NQDs. As a result data points of Fig. 2(d) measured for g-NQDs coupled to the metal film (diamonds) and reference g-NQDs (circles) merge when the PL lifetime is ~10 ns.

Our modeling also shows that the increase in β leads to the reduction of R_0. Therefore, in NQDs with very efficient AR, R_0 never exceeds unity (see Fig. 4(a); calculation for $\beta \geq 14$). This result

explains why only a moderate metal-induced enhancement of R_0 with values <1 was observed in earlier studies conducted on standard [20,21] and intermediate-shell (~10 ML) NQDs [22] in which AR was not significantly suppressed (initial $Q_{2X} < 0.2$). Although the decrease of β due to plasmonic enhancement of biexciton radiative recombination can explain increases of R_0 in these studies [20,22], our analysis shows that metal-induced quenching with a rate that scales linearly with j is necessary to explain the values of R_0 greater than unity.

Usually, metal quenching of fluorophores has been attributed to Förster type energy transfer (ET) [3]. In the case of multiexcitons, this process is expected to exhibit the same j^2 scaling as radiative decay (see SI. 6). Therefore, photon bunching is not possible if metal-induced PL quenching is dominated by ET to the metal. Alternatively, nonradiative recombination via intra-gap recombination centers (Fig. 4(c)) or charge tunneling into the proximal metal (Fig. 4(d)) can lead to PL quenching with a desired linear scaling (see SI. 7 and SI. 8). Nonradiative recombination via intra-gap defects has been often invoked in various models of quantum dot blinking [23,24]. It is feasible that coupling to MN introduces new defect states at the metal-ligand or metal-NQD interface, which could provide new recombination pathways as illustrated in Fig. 4(c) [25]. Analysis in SI. 8 shows that this process will result in PL quenching with desired linear scaling, independent of whether this band is fully or partially occupied.

In the case of a proximal MN, the metal itself can serve as a recombination band if its Fermi level is located within the NQD band gap region [26]. Tunneling of carriers from standard NQDs to the metal on the other hand has been proved to be slow due to the barrier presented by the organic ligand [27]. However, unlike standard NQDs, which are more rounded in shape, g-NQDs in general show more clear hexagonal facets [14]. We surmise that ligand coverage on such particles is likely to be non-uniform as a result of differing interactions with chemically distinct

facets. Efficient tunneling can therefore occur in some g-NQD through the regions of lesser ligand coverage. This picture could also explain the variation of α that in turn leads to wide distribution of the R_0 values (Figs. 2(c) and 2(d)).

Next we analyze the pump-intensity dependence of R (Fig. 3(d)) using the model described in SI. 2. We first calculate R vs. $\langle N \rangle$ for a reference g-NQD with $Q_{1X} = 1$ (i.e., $\alpha = 0$), assuming that AR is the only nonradiative decay channel ($\beta = 36$, which corresponds to $Q_{2X} = 0.1$). The calculated trace (Fig. 4(b), squares) reproduces the trend observed for the reference dot (Fig. 3(d), triangles). For g-NQDs on silver films, we set $\gamma = 1$ (as suggested by our analysis) and calculate R vs. $\langle N \rangle$ for the same combinations of α and β values as in Fig. 4(a). When $\alpha >> 1$, the maximum value of R is ~2 at $\langle N \rangle < 0.1$ and it decreases with increasing $\langle N \rangle$ until it approaches unity for $\langle N \rangle >> 1$ (Fig. 4(b), black solid line). The decrease is monotonic and the key features reported in Fig. 3d, namely, transition towards antibunching ($R < 1$) regime and a minimum (a "dip") near $\langle N \rangle \sim 0.2$ - 0.3 are not reproduced. When α is reduced and β is kept zero, R is also reduced, however, it still shows a similar monotonic decrease with $\langle N \rangle$. Interestingly, the "dip" feature can be reproduced only if we assume a *nonzero* rate of AR (Fig. 4(b)) [28]. These calculations together with our previous analysis lead to the conclusion that while R_0 of ~2 can be reached under the condition of metal-induced quenching dominating over both radiative and AR processes, the interplay between all of the decay processes must be considered to explain the pump intensity dependence of R. Finally we note that we have neglected the possibility of NQD charging due to photo-ionization in these analyses. In SI. 9 we show that charging can alone cannot explain the observations of $R_0 > 1$.

In summary, our study provides evidences that photon emission statistic of individual NQDs can

be modified by multiexciton-MN interactions. Note that although this modification is realized through the reduction in quantum yields of single as well as the multiexciton states, dramatic shortening of PL lifetime down to sub-nano second will allow driving of the system with a repetition rate up to 1 GHz. This is highly desirable for any technological applications [29]. Finally, we would like to point out that our study provides a first glimpse into the effect of MNs on radiative and nonradiative recombination processes of multiexcitons, which would open new plasmonic route to manipulate multiexciton processes.

Acknowledgements This work was conducted, in part, at the Center for Integrated Nanotechnologies (CINT), a U.S. Department of Energy, Office of Basic Energy Sciences (OBES) user facility. Y.-S.P. is supported by CINT. Y.G., Y.C. and A. P. acknowledge Los Alamos National Laboratory Directed Research and Development Funds. V.I.K. is supported by the Chemical Sciences, Biosciences and Geosciences Division of OBES, Office of Science, U.S. DOE. H.H. and J.A.H. acknowledge a Single-Investigator Small-Group Research Award (2009LANL1096), OBES, OS, U.S. DOE.

Author Information Correspondence and requests for materials should be addressed to H.H. (htoon@lanl.gov), A.P. (apiryat@lanl.gov), and V.I.K. (klimov@lanl.gov).

[1] J. A. Schuller *et al.*, Nature Mater. **9**, 193 (2010).
[2] K. Munechika *et al.*, Nano Lett. **10**, 2598 (2010).
[3] K. T. Shimizu, W. K. Woo, B. R. Fisher, H. J. Eisler, and M. G. Bawendi, Phys. Rev. Lett. **89**, 117401 (2002).
[4] Y. Ito, K. Matsuda, and Y. Kanemitsu, Phys. Rev. B **75**, 033309 (2007).
[5] C. T. Yuan, P. Yu, H. C. Ko, J. Huang, and J. Tang, ACS Nano **3**, 3051 (2009).
[6] Y.-S. Park *et al.*, Phys. Rev. Lett. **106**, 187401 (2011).
[7] G. Nair, J. Zhao, and M. G. Bawendi, Nano Lett. **11**, 1136 (2011).
[8] P. Michler *et al.*, Nature **406,** 968 (2000).
[9] A. Högele, C. Galland, M. Winger, and A. Imamoğlu, Phys. Rev. Lett. **100,** 217401 (2008).
[10] T. Basché, W. E. Moerner, M. Orrit, and H. Talon, Phys. Rev. Lett. **69,** 1516 (1992).
[11] C. H. Bennett and D. P. DiVincenzo, Nature **404,** 247 (2000).
[12] V. I. Klimov *et al.*, Science **290,** 314 (2000).
[13] Y. Chen et al., J. Am. Chem. Soc. **130,** 5026 (2008).
[14] F. García-Santamaría *et al.*, Nano Lett. **11,** 687 (2011).
[15] F. García-Santamaría *et al.*, Nano Lett. **9,** 3482 (2009).
[16] N. H. Mack et al., Langmuir **27,** 4979 (2011).
[17] As a first order approximation, we calcualte $\langle N \rangle$ without considering the plasmonic enhancement of absorption cross-section.
[18] J. A. McGuire *et al.*, ACS Nano **4,** 6087 (2010).
[19] J. A. McGuire, J.Joo, J. M. Pietryga, R. D. Schaller, and V. I. Klimov, Acc. Chem. Res. **41,** 1810 (2008).
[20] H. Naiki, S. Masuo, S. Machida, and A. Itaya, J. Phys. Chem. C **115,** 23299 (2011).
[21] S. Masuo, H. Naiki, S. Machida, and A. Itaya, Appl. Phys. Lett. **95,** 193106 (2009).
[22] D. Canneson *et al.*, Phys. Rev. B **84,** 245423 (2011).
[23] C. Galland *et al.*, Nature **479,** 203 (2011).
[24] P. A. Frantsuzov, S. Volkán-Kacsó, and B. Jankó, Phys. Rev. Lett. **103,** 207402 (2009).
[25] P. Nagpal and V. I. Klimov, Nature Commun. **2,** 486 (2011).
[26] Fermi level of sliver indeed lies at the middle of CdSe band gap.
[27] T. D. Krauss, S. O'Brien, and L. E. Brus, J. Phys. Chem. B **105,** 1725 (2001).
[28] The dip is reproduced at $\langle N \rangle \sim 2$ while it appears at $\langle N \rangle$ of 0.3-0.4 in the experimental data of Fig. 3 (c). This difference may result from the enhancement of absorptioin cross-section.
[29] In contrast, g-NQDs can only be driven at MHz repetition rates due to their slow decay >50ns.

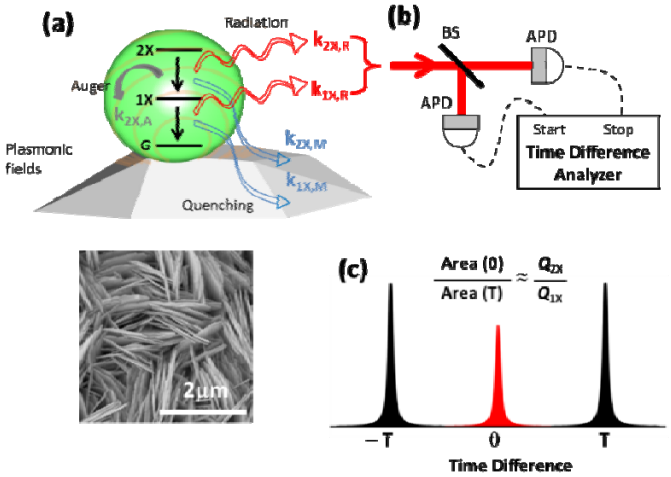

Aspect Ratio = 1.35

FIG. 1. (a) Schematics of a biexciton (2X) → exciton (1X) → ground state (G) quantum cascade process of an NQD coupled to the rough silver surface (scanning electron microscopy image in the lower left corner). (b) Hanbury Brown and Twiss setup consists of a 50/50 beam splitter (BS) and two avalanche photodiodes (APDs). (c) Second-order photon correlation function $g^{(2)}(t)$ measured under pulsed excitation without any spectral selection. The area of the central peak ($g^{(2)}(t = 0)$) measures the probability of creating 2X and subsequent emission of two photons via the quantum cascade process and can be expressed as $g^{(2)}(0) \approx Q_{2X} Q_{1X} \langle N \rangle^2$ for $\langle N \rangle \rightarrow 0$ limit. The area of the side peak ($g^{(2)}(t = T)$; T is the separation between sequential laser pulses) reflects the probability of exciton generation and emission in two successive excitation cycles and can be expressed as $g^{(2)}(T) \approx (Q_{1X} \langle N \rangle)^2$. Consequently, the degree of photon bunching given by $R = g^{(2)}(0)/g^{(2)}(T)$ approaches $R_0 \approx Q_{2X}/Q_{1X}$ when $\langle N \rangle \rightarrow 0$.

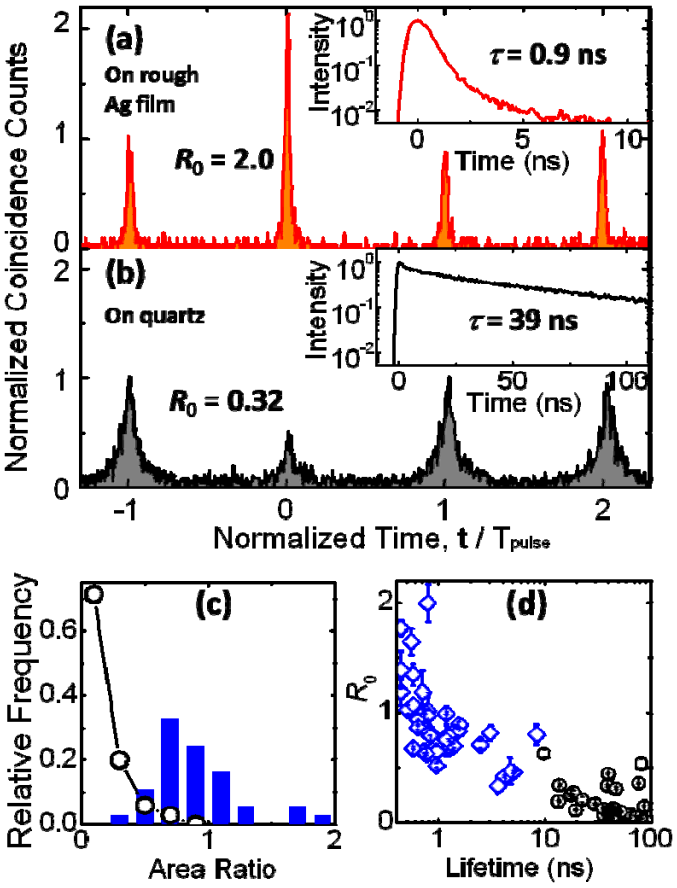

Aspect Ratio = 0.76

FIG. 2. $g^{(2)}$ functions of single g-NQDs deposited (a) on a rough silver surface and (b) on a quartz substrate. Insets in (a) and (b) display PL decay of each corresponding g-NQD. (c) Histograms of normalized zero-delay-peak areas measured for 35 g-NQDs on the quartz (open circles) and 37 g-NQDs on the rough silver film (blue bar). (d) The plot of R_0 vs. average PL lifetime (diamonds: g-NQDs on the silver film; circles: reference g-NQDs).

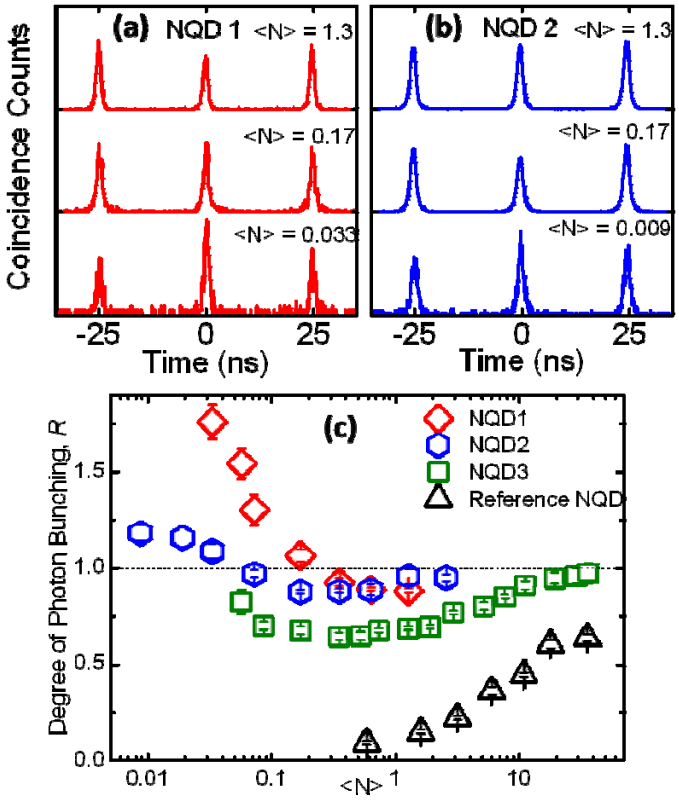

Aspect Ratio = 0.84

FIG. 3. (a)-(b) $g^{(2)}$ functions of two g-NQDs on a rough silver film acquired at different pump powers. (c) Pump power dependence of R of three NQDs and a reference NQD plotted as a function of $\langle N \rangle$.

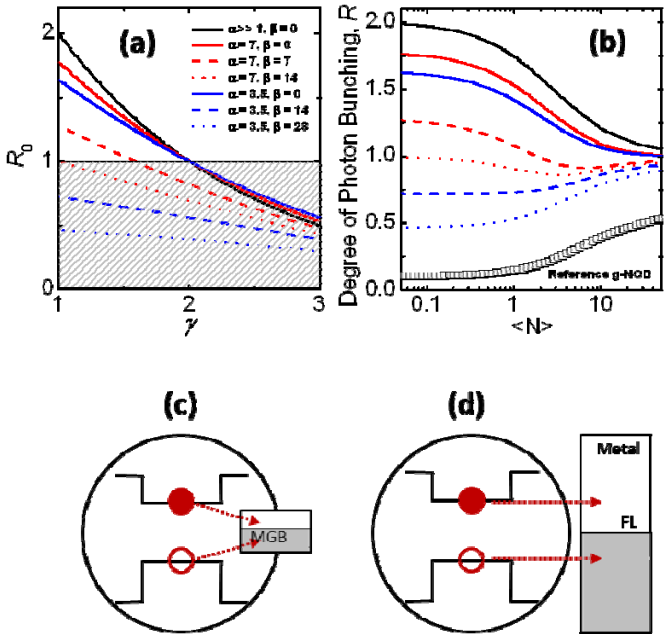

Aspect Ratio = 1.05

FIG. 4. (a) Calculations of R_0 vs. γ for various values of α and β (indicated in the figure). α value of 7 is selected based on ~ 8 fold reduction of the g-NQD quantum yield reported in Fig.S3. (b) Simulations of R vs. $\langle N \rangle$ for $\gamma = 1$ and different values of α and β (same as in (a) using the same line styles and colors). Squares: calculated trace for a reference g-NQD. Schematic for rapid recombination via (c) trap states forming a MGB and (d) uncorrelated tunneling of electrons and holes into the metal (d).